# 4

# Quantification of dynamical heterogeneities of hydration water in lipid membrane above supercooling

## 4.1 INTRODUCTION

In biological systems, water is confined between molecular assemblies where water dynamics is relevant in membrane functioning and cytoskeletal organizations [Munro, 2003; Lingwood and Simons, 2010; Jungwirth, 2015]. In the last decade, with a major advancement in computer simulation and experimental techniques, water near soft interfaces are found to have very slow relaxation times [Pal *et al.*, 2002; Balasubramanian *et al.*, 2002; Ji *et al.*, 2010; Biswas *et al.*, 2013; Das *et al.*, 2015]. Recently, protein displacements in live cell membranes are found to have robust exponential tails due to the underlying dynamical heterogeneities [Gowrishankar *et al.*, 2012; He *et al.*, 2016].

The nano scale heterogeneity in membrane dynamics is believed to play the dominant role in various cellular processes such as signal transduction, matter transport and enzymatic activities in cells [Mouritsen and Jørgensen, 1992]. Dynamical heterogeneities in fluid membranes are observed on the scale of $80 - 150$ nm with super-resolution stimulated emission depletion microscopic and fluorescence correlation spectroscopic techniques, even in absence of cholesterol [Roobala and K., 2017]. Hydration dynamics has been identified as a sensitive ruler to determine membrane associated protein structure, topology, immersion depth and so on using $1H$ Overhauser dynamic nuclear polarization (ODNP)-enhanced NMR relaxometry [Cheng *et al.*, 2013]. However, time dependent Stoke shift experiments are found not to be suitable for measuring hydration dynamics near proteins due to excess contributions from protein motions [Heid and Braun, 2019]. Large signal acquisition time is required for signal detections below single monolayer coverage by conventional vibrational sum frequency generation (VSFG) spectroscopy. To overcome these limitations, heterodyning is used to shift one frequency range into another [Stiopkin *et al.*, 2008] and thus it has revealed that that hydrogen bond dynamics near a membrane is highly dependent on the water dynamics through a hydrogen bond network rather than hydrogen bonding near a specific interaction site [Inoue *et al.*, 2017]. Combining 2D HD-VSFG spectroscopy and molecular dynamics simulations, it has been found that water dynamics has a transition from interface like to bulk-like behavior at $\sim 7$ Å away from phosphatidylcholine monolayer interface [Roy *et al.*, 2014]. Structural heterogeneity of interfacial water has been reported near negatively, positively and charged lipid/surfactant interfaces using time-resolved sum-frequency generation spectroscopy [Cyran *et al.*, 2018].

Experimental method to extract length scale of spatial correlations in colloidal system is still inconclusive since the exact relation between correlations and length scale is unknown [Hagamanasa *et al.*, 2015; Zhang and Cheng, 2016]. The influence of hydration layers on global dynamics of proteins is debated [Chen *et al.*, 2006; Persson and Halle, 2008; Schiró *et al.*, 2015; Nandi *et al.*, 2017].

Complementary to experiments, simulation data provide accessibility to atomic trajectories which can be directly used to extract relaxation time scales of water near soft interfaces. Water confined near silica hydrophilic pores at room temperature reveals two different dynamical regimes similar to supercooled bulk water [Gallo *et al.*, 2000a,b]. Confined diffusion of nano-particles is found to follow non-Gaussian statistics even at the long time Brownian stage [Xue *et al.*, 2016]. Intermittency in solute motion has been identified as the source of non-Gaussian behavior where solute solvent dynamics are decoupled [Acharya *et al.*, 2017]. Distinct heterogeneous water dynamics have been found for four dynamically connected water layers [Das *et al.*, 2013]. Dynamics and thermodynamics

of interface water near a bilayer are found to be correlated with the phases of the bilayers [Debnath *et al.*, 2013]. Chemical heterogeneity in a lipid bilayer does not immediately imply dynamic heterogeneity. Different mobility groups are found for lipid membranes in an $L_\beta$ phase where characteristics time and length scales are identified to be $1-2$ $\mu$s and $1-10$ nm which can couple to biomolecules in the membrane [Shafique *et al.*, 2016]. Simple polydisperse systems with continuously varying diameters of particles show dynamic heterogeneity only at low temperatures and not at high temperatures [Russo and Tanaka, 2015; Tah *et al.*, 2018]. Recently it has been shown that such small scale fluctuations of membranes originating from the longitudinal component of lipid orientations can be used in deriving the bending modulus or curvature of the membrane where the tilt moduli can be obtained from transverse components of lipid orientations [Watson *et al.*, 2012; Terzi and Deserno, 2017; Chaurasia *et al.*, 2018]. Increased viscosity at the interface is found to be the source of slowed diffusion of proteins than in bulk [Pronk *et al.*, 2014]. $20-50\%$ faster water diffusion is obtained for disordered surfactant membranes compared to the ordered ones [McDaniel and Yethiraj, 2017]. Long term correlation and sub-diffusion of lipid recognition protein with the membrane are the contributing factors in enhancing the probability of encountering the target complex on the membrane surface [Yamamoto *et al.*, 2015]. The pertinent question remains, (i) what are the sources of distinct dynamics of confined water at room temperature? [Sciortino *et al.*, 1996; Gallo *et al.*, 1996; Bellissent-Funel, 1998; Mazza *et al.*, 2006; Jana and Bagchi, 2009; Youssef *et al.*, 2011] (ii) Can the dynamical heterogeneity length scale be predicted for confined water near membranes? This leads an open question: can the length scale be tunable from the membrane phase?

In this chapter, we use all atom molecular dynamics simulations for a fully hydrated lipid bilayer to identify chemically confined interface water molecules which form hydrogen bonds to lipid heads. Translational mean square displacements, non-Gaussian parameters and van Hove auto-correlation functions are calculated to understand if chemically confined water near DMPC lipid head-groups exhibits dynamical heterogeneity at temperature (308 K) well above supercooling. Wave-length dependence of self intermediate scattering functions of interface and bulk water are calculated. Heterogeneous relaxation time scales present in the interface water are quantified and their dependence on chemical confinement is examined. Block analysis is employed on the interface and van Hove correlation functions are calculated for interface water by varying the block sizes. The dynamical heterogeneity length-scale of interface water is quantified from the block analysis and its relation with the membrane curvature is examined by calculating the Fourier transform of tilt angle fluctuations of lipid molecules. The influence of chemical nature of lipid chains and physical properties of the lipid bilayer on the heterogeneous dynamics of interface water is systematically analyzed to find out the origin of the slow relaxation rates of interface water molecules. Our calculations provide the microscopic mechanism responsible for such a behavior at room temperature with their implications and potential applications. We attempt to predict the dynamical heterogeneity length scale of confined water and its relation to the properties of the membranes.

## 4.2 SIMULATION DETAILS

An all atom molecular dynamics simulation is carried out for 128 DMPC molecules in the presence of 5743 TIP4P/2005 water molecules at its fully hydrated state [Lopez *et al.*, 2004; Zhao *et al.*, 2008; Trapp *et al.*, 2010] using a previously equilibrated DMPC system at 308 K [Srivastava and Debnath, 2018]. Force field parameters for DMPC are obtained using Berger united atom force field [Berger *et al.*, 1997; Cordomí *et al.*, 2012] which are used in conjunction with a TIP4P/2005 [Abascal and Vega, 2005] water model. The specific combination of the force-fields of water and the bilayer is found to reproduce the experimental dynamical properties of water keeping the membrane fluid phase intact [Srivastava *et al.*, 2019b]. Moreover, force-fields will not alter the underlying mechanism of dynamical heterogeneity of confined water near membranes compared to that of the bulk water as seen for many glass-former liquids [Wong and Faller, 2007; Srivastava and Voth,

2013; He and Maibaum, 2017]. Area per head-group, bilayer thickness and order parameter for the DMPC bilayer using the force-fields match well with the experimental data [Petrache *et al.*, 2000; Aussenac *et al.*, 2003; Gurtovenko *et al.*, 2004; Kučerka *et al.*, 2011; Srivastava *et al.*, 2019b] implying suitability of the TIP4P/2005 force field with the Berger united atom force field.
An NPT run is carried out for 100 ns with a 2 fs time step. The system is equilibrated at 308 K using a velocity rescaling method [Bussi *et al.*, 2007] with a coupling constant of 0.5 ps. The pressure is maintained at 1 bar using semi-isotropic pressure coupling by the Berendsen pressure coupling method [Berendsen *et al.*, 1984b] with a coupling constant of 0.1 ps. Coulombic and van der Waals interactions are cutoff at 1 nm. Long range interactions are corrected using the particle mesh Ewald [Darden *et al.*, 1993; Essmann *et al.*, 1995b; Allen and Tildesley, 1987] method with a 0.12 nm grid size. All bonds are constrained using the LINCS [Hess *et al.*, 1997] algorithm. Periodic boundary conditions are applied in all three directions. Next an NVT simulation is performed for 1.9 ns with a 0.4 fs time step where the last 1 ns run is analyzed for water dynamics. 1 ns run-length is found to be long enough to obtain adequate sampling to calculate the relaxations discussed in the study. Parameters for temperature coupling, cutoff distances and long range interactions are kept the same as in the previous run. Trajectories are collected at every 10 fs. The simulation box-length for the hydrated DMPC lipid is 6.24 nm along the x and y directions and 7.95 nm along the z direction.
For investigating the length-scale associated with dynamical heterogeneities, the hydrated DMPC water system is replicated 4 times using the same set of parameters as for the smaller system. Thus a bilayer of 512 DMPC lipids is simulated, which is known to be large enough to calculate lipid small length scale fluctuations from their tilt [Watson *et al.*, 2012]. An NPT equilibration run is carried out for 100 ns followed by a 2 ns NVT run with the same time step and saving frequency as for smaller systems. All other parameters are kept the same as the smaller system. Simulation box length for the larger system is 12.63 $nm^2$ both along the x and y directions and 7.76 nm along the z direction. Since the 12.63 $nm^2$ all atom DMPC-water system is computationally very expensive and the long time relaxation of the interface water molecules in the 6.24 $nm^2$ bilayer is 1 ns, the last 1 ns trajectory of the 12.63 $nm^2$ membrane is used for the production run. For the analysis of spectral intensity from lipid tilts, the same trajectory is used. To compare the dynamics of interfacial water with bulk water molecules (BW), a 2 ns NPT run followed by a 400 ps NVT run is carried out for a box of only 851 TIP4P/2005 water molecules using the same parameters as in a DMPC-water system. Equilibration of the system is checked and the last 100 ps data are analyzed for BW since BW relax much faster than the interface water. The box length of BW is 3.69 nm along the x and y directions and 1.84 nm along the z direction. All simulations are carried out using GROMACS 4.6.5 [Bekker *et al.*, 1993; Berendsen *et al.*, 1995; Lindahl *et al.*, 2001; Spoel *et al.*, 2005; Hess *et al.*, 2008; D. van der Spoel and the GROMACS development team., 2013]. All analyses are performed using in-house fortran codes.

## 4.3 DEFINITION OF DIFFERENT CLASSES OF INTERFACE WATER

Figure 2.1 in the previous chapter show the bilayer and a single DMPC molecule present in the bilayer respectively. To decouple the contribution of bulk water molecules (BW) to the dynamical properties of hydration layers, interface water is classified based on geometric definitions. If a water molecule continuously resides in a layer which is ±3 Å (the first hydration layer obtained from g(r) of $O_{water}$-$N_{lipid}$ and O-O of water in figure 2.6) away from the location of the nitrogen head group density of DMPC for a 100 ps time window, the molecule is identified as an interface water molecule (IW) [Srivastava and Debnath, 2018]. The definition of IW considers most of the IW molecules forming hydrogen bonds to oxygen atoms of glycerol, carbonyl, and phosphate head groups of DMPC [Srivastava and Debnath, 2018; Srivastava *et al.*, 2019b]. The 100 ps time window is chosen from the residence time of interface water molecules for a 1 ns time window (figure 2.7 and table 2.4). Similar residence time was found earlier for interface water near a DPPC bilayer using an SPC water model [Debnath *et al.*, 2010]. Since IW molecules reside in the hydration

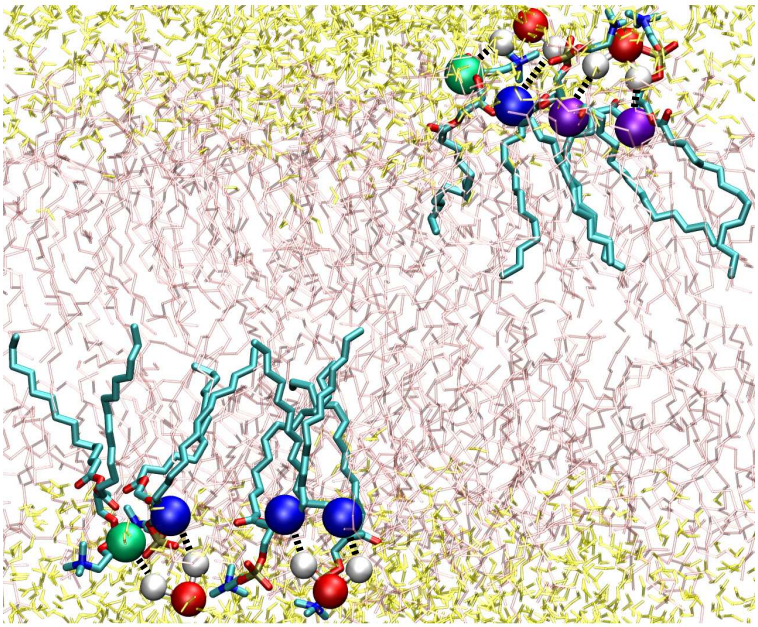

Figure 4.1: Interface water continuously residing for 400 ps ($IW_{CR400}$) in the first hydration layer of DMPC. Color code: Blue vdw - carbonyl oxygen; Violet vdw - glycerol oxygen; water molecules were shown in CPK. DMPC bilayer shown in transparent in pink licorice representation.

layer continuously for the 100 ps time window, the time window is referred to as their confinement lifetime for further discussion. To check the effect of confinement lifetime on IW molecule relaxation, another class of IW molecules is chosen which stay continuously in the hydration layer for 400 ps and is referred to as $IW_{CR400}$. Figure 4.1 show the location of $IW_{CR400}$ hydrogen bonded to carbonyl, glycerol and phosphate oxygens for the entire 400 ps. Furthermore, to check the influence of lipid head moieties on the relaxation time-scales of IW, different classes of IW molecules are identified. If one IW molecule of 100 ps confinement lifetime is hydrogen bonded ($r_{O-O} < 0.35$ nm and $\theta_{HOO} < 30^o$) to another IW molecule of the same lifetime, it is referred to as IW-IW. Additionally, if an IW molecule is hydrogen bonded to the carbonyl (CO), phosphate (PO) or glycerol (Glyc) moiety of lipid heads (shown in different colors in figure 2.1 a)), the IW molecule is referred to as IW-CO, IW-PO or IW-Glyc respectively [Srivastava and Debnath, 2018]. Note, these different classes of IW molecules are hydrogen bonded for at least a single time frame during the 100 ps confinement lifetime and thus are allowed to exchange their partners within the observation period.

## 4.4 TRANSLATIONAL MEAN SQUARE DISPLACEMENT

To analyze the dynamical nature of bound waters, translational mean square displacement (MSD) is calculated in 3 dimensions for all classes of water using the equation 2.1. Figure 4.2 shows that the BW molecules follow diffusive behavior at longer time where all classes of IW remain sub-diffusive due to the trapping in a cage formed by the neighboring hydrogen bond networks. $MSD_z$ is slower than $MSD_{xy}$ (figure 4.4). The nature of the MSD of IW molecules does not coincide with the one followed by the lipid head groups, so the translational displacements of lipid heads are not straight forwardly coupled to that of the IW molecules. $IW_{CR400}$ exhibits the slowest MSD due to longer confinement lifetime compared to the other classes of IW revealing that the confinement lifetime has an influence on the slowest translational dynamics of IW.

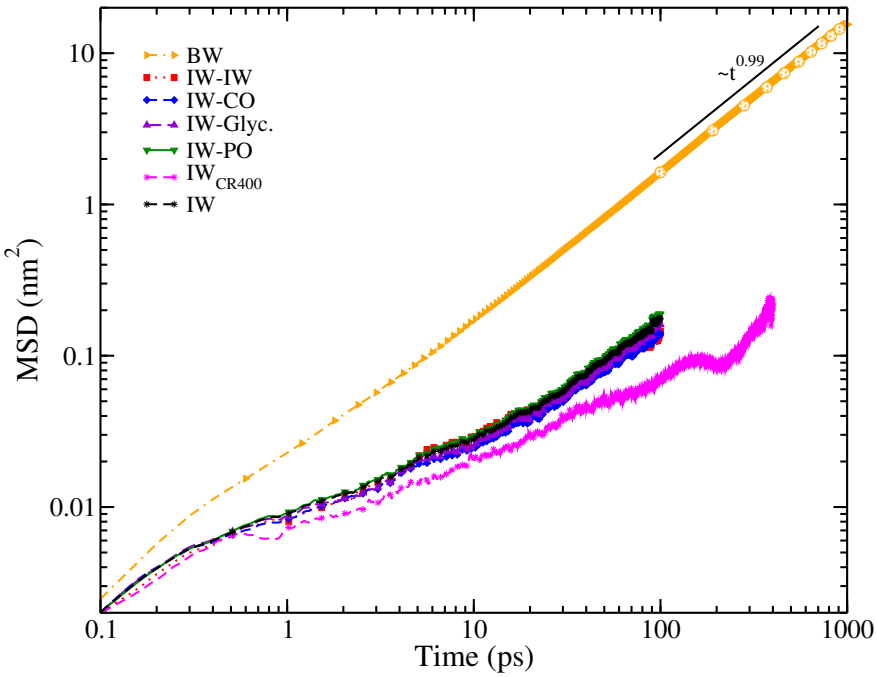


Figure 4.2: Translational mean square displacement for all classes of IW and BW. All classes of IW follow sub-diffusive regime while BW obeys diffusive regime with diffusion exponent as $\alpha = 0.99$.

## 4.5 NON-GAUSSIAN PARAMETER

To understand the origin of the subdiffusive nature of the IW, a non-Gaussian parameter (NGP, $\alpha_2$(t)) [Shell *et al.*, 2005; Hansen and McDonald, 2006] is calculated in three dimensions using the equation 2.10. The NGP for the BW decays asymptotically to zero through a maximum confirming the Gaussian diffusion (figure 4.3). The values of NGP for different classes of IW start increasing to much higher amplitudes than that for the BW and reach a maximum between $\beta$ and $\alpha$-relaxation time scales. Respective relaxation time-scales, $\tau_{\alpha_2}$, are mentioned in table 4.1. The slow decays of the NGP for IW molecules are due to the release of the IW molecules from the respective cages via diffusion. Earlier it has been found that $\tau_{\alpha_2}$ characterizes the correlation timescale of spatially heterogeneous motion for polymer melts and can feature diffusive time-scale [Starr *et al.*, 2013]. The peak of NGP along z appears at a longer time-scale than that along xy. The peak locations of NGP ($\tau_{\alpha_2}$) are consistent with the confinement lifetime of 100 ps (figure 4.4 c) and d)).

Similar cross-over from cage to translational diffusive regime at the time scale of $\tau_{\alpha_2}$ are found for Brownian particles in a periodic effective field [Vorselaars *et al.*, 2007]. Since IW molecules leave the layer after their confinement lifetimes of $\sim$ 100 ps, the maxima of their respective NGP are nearly at 100 ps (table 4.1). IW-Glyc being buried in the hydrophobic core of the lipid membrane (figure 2.1 a)) show the highest $\tau_{\alpha_2}$ relaxation among IW molecules which are continuously residing for 100 ps. Interestingly, IW$_{\mathrm{CR400}}$ exhibits very strong non-Gaussian behavior for a longer period of time compared to other classes of IW molecules and decay after $\sim$ 340 ps which is again closer to their confinement lifetimes. The slow relaxations of all classes of IW molecules signify a strong structural arrest by their surrounding molecules similar to supercooled liquids exhibiting dynamical heterogeneity [Kob *et al.*, 1997; Vorselaars *et al.*, 2007; Youssef *et al.*, 2011]. The transition from the $\beta$ to the $\alpha$-relaxation occurs at a similar spatio-temporal scale where the respective MSD have transition from the sub-diffusive to the diffusive regime.

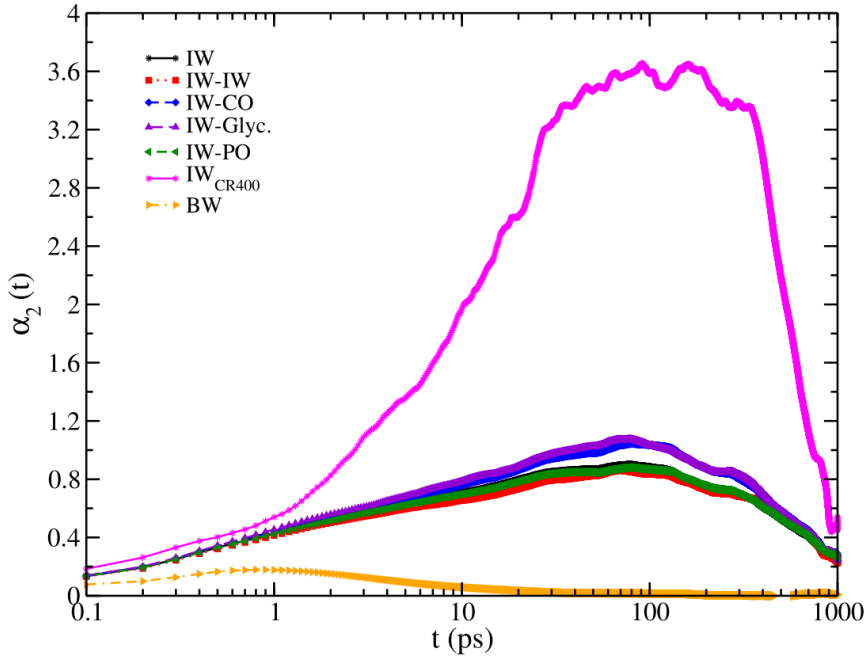


Figure 4.3: NGP ($\alpha_2$(t)) for all classes of IW molecules and the BW molecules show a cross-over from $\beta$ to $\alpha$ relaxation at the same time-scale when respective mean square displacements have transitions from sub-diffusive to diffusive region.

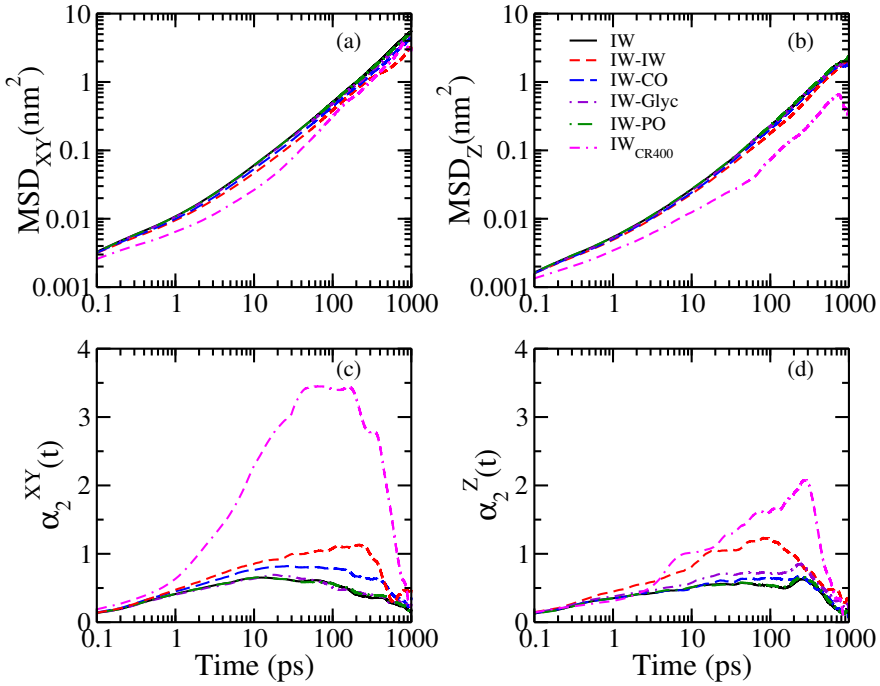


Figure 4.4: Translational mean square displacement for all classes of IW molecules along a) xy, b) z. NGP for all classes of IW molecules along c) xy and d) z.

Table 4.1: Relaxation time scales ($\tau_{\alpha_2}$) for all classes of IW and BW corresponding to peak of NGP.

| Region | $\tau_{\alpha_2}$ (ps) |
|---|---|
| IW | 78.70 |
| IW-IW | 70.10 |
| IW-CO | 80.10 |
| IW-Glyc. | 82.80 |
| IW-PO | 78.40 |
| $IW_{CR400}$ | 344.80 |
| BW | 0.90 |

## 4.6 VAN HOVE CORRELATION FUNCTION

For gaining deeper insights into the dynamical evolution of IW molecules associated with lipid moieties, the self part of the radial van Hove correlation function [Hopkins *et al.*, 2010] is calculated using the equation 1.1. Figure 4.5 shows the radial van Hove correlation function with a time interval (table 4.1) corresponding to the $\tau_{\alpha_2}$-relaxation of NGP where the dynamical heterogeneity is most significant for all classes of water. All classes of IW molecules show very strong deviations from Gaussianity where the BW follow Gaussian behavior. Due to the chemical confinement of different classes of IW in the vicinity of lipid heads, there is a strong correlation pertaining to longer length-scales which decays at a smaller length scale for the BW. Among different classes of IW, the van Hove correlation function of IW-Glyc which is buried towards the membrane core has the maximum amplitude depicting highest extent of correlation consistent with the highest correlation obtained from the respective NGP. Importantly, the van Hove correlation function of $IW_{CR400}$ has two peaks and a shoulder unlike other classes of IW and their correlations decay at a smaller length scale than that for other classes of IW. Since $IW_{CR400}$ has a larger time-window of 400 ps as the confinement lifetime, small numbers of $IW_{CR400}$ are found on the bilayer surface which are inhomogeneously clustered on the bilayer surface. This might result in rattling or hopping of $IW_{CR400}$ between cages which are not closely spaced on the bilayer surface unlike other classes of IW.

Since the bilayer is symmetric along the x and y directions where xy is the bilayer surface, one dimensional van Hove correlation function is calculated for all classes of water molecules along one of the directions to get a better description of deviations from Gaussianity. Figure 4.6 represents one dimensional van Hove correlation functions for time intervals corresponding to the same $MSD_{xy}$ for all water molecules in the sub-diffusive regime. The time intervals used in the calculations are 5.12 ps, 5.2 ps, 6.74 ps, 5.51 ps, 5.01 ps, 5.12 ps and 0.9 ps for IW, IW-IW, IW-CO, IW-Glyc, IW-PO, $IW_{CR400}$ and BW respectively. BW follow Gaussian dynamics and all classes of IW molecules show larger deviations from Gaussianity which have been manifested as an established behavior of dynamical heterogeneity in supercooled glass forming liquids [Chaudhuri *et al.*, 2007; Sengupta and Karmakar, 2014]. The origin of exponential tails for the IW molecules is the waiting time distributions for the subsequent jumps or hopping transitions between cages formed by the neighboring hydrogen bond networks.

## 4.7 SELF INTERMEDIATE SCATTERING FUNCTION

Since self intermediate scattering function (SISF, $F_s(q,t)$) is another universal feature of dynamical heterogeneity and the bilayer surface (xy plane) is symmetric along the x and y directions, two dimensional $F_s(q,t)$) is calculated using equation 1.2. Here $q = \frac{2\pi}{\lambda}$ where $\lambda$ is the wavelength.

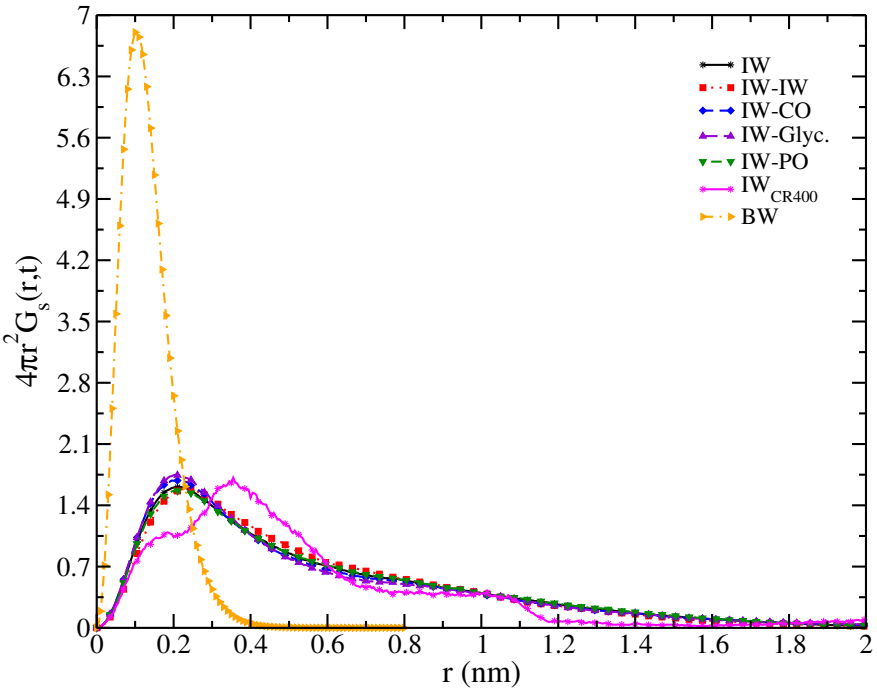


Figure 4.5: Self part of translational radial van Hove correlation function for all classes of IW and BW. The existence of larger correlation length indicates structured network of IW than BW.

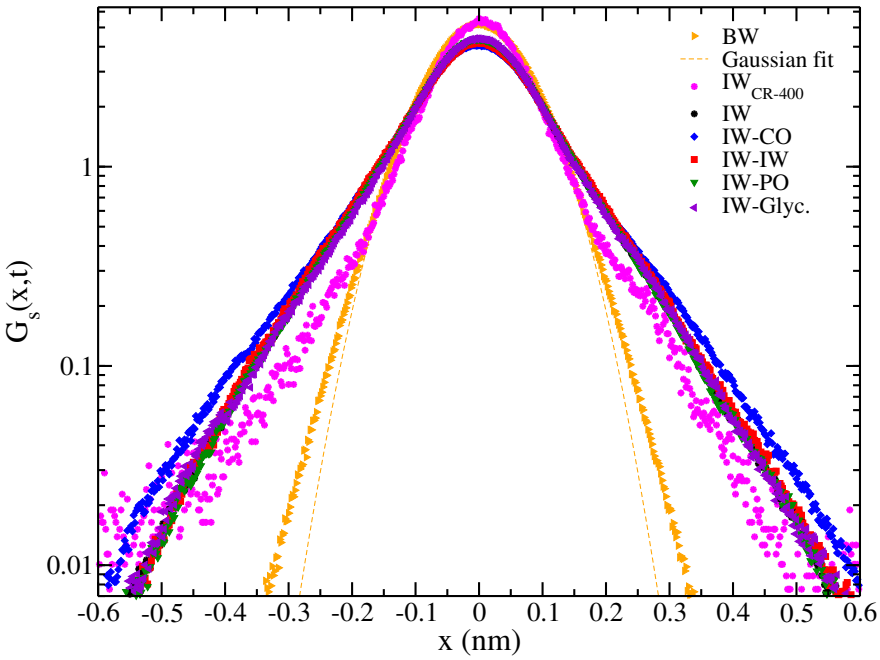


Figure 4.6: Self part of van Hove correlation function along x direction. Gaussian fitting for BW depicts Fickian dynamics while non-exponential tails for all classes of IW reveal deviations from Gaussian behavior.

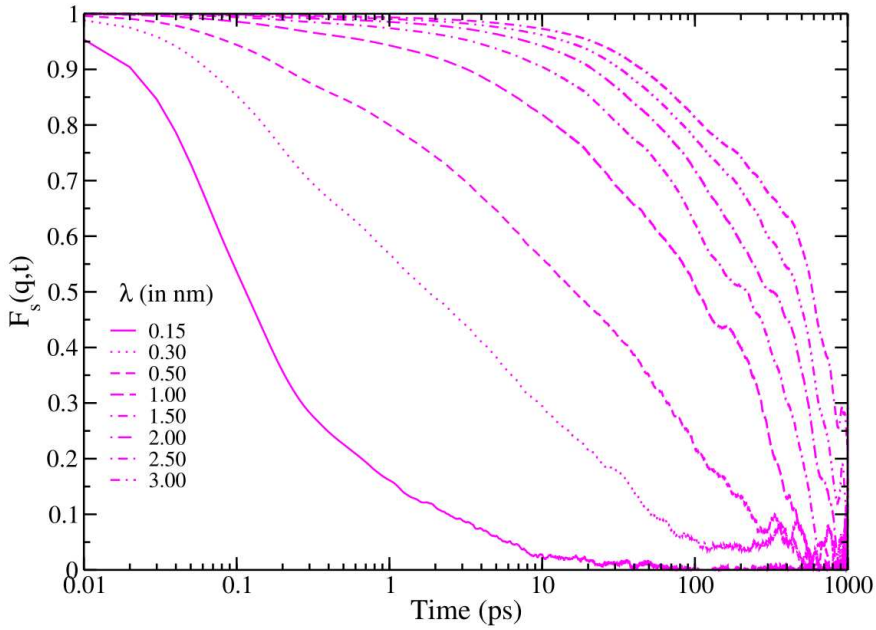


Figure 4.7: SISF of $IW_{CR400}$ at $\lambda$ values ranging from 0.50 nm to 3.00 nm.

To obtain the wave-vector dependence on the $\alpha$-relaxation times, SISF are calculated at different values of $\lambda$. Figure 4.7 and 4.8 show the behavior of SISF at different $\lambda$ for the $IW_{CR400}$ and the BW.

Although the $\beta$ and $\alpha$-relaxation times of the IW molecules and the BW are not prominently disparate by characteristic Boson peaks as observed for the supercooled liquids [Hansen and McDonald, 2006], SISF very clearly scales up in different time regimes: very fast ballistic motion in a cage, cage relaxations and slow escape from the cage. Our BW data are fitted best to two relaxation time-scales using,

$$F_s(q,t) = (1 - f_Q)exp\Big( - \Big(\frac{t}{\tau_s}\Big)^2\Big) + f_Q exp\Big( - \Big(\frac{t}{\tau_\alpha}\Big)^{\beta_\alpha}\Big) \tag{4.1}$$

$f_Q$ is known as the Debye-Waller factor, $\tau_s$ is the time-scale for ballistic motion and $\tau_\alpha$ is the relaxation time-scale of the cage [Magno and Gallo, 2011]. The stretched exponential in the equation is known as the Kohlrausch-William-Watt (KWW) function [Camisasca *et al.*, 2016] where $\beta_\alpha$ can be correlated with the breakdown of the Stokes-Einstein relation for supercooled liquids [Bhowmik *et al.*, 2016]. Preservation or violation of the Stokes-Einstein equation has been calculated for the BW from its temperature dependence where the immobile component is characterized by slower $\tau_\alpha$ and fast moving particles are characterized by $\tau_{\alpha_2}$ [Kawasaki and Kim, 2017]. However, to establish such preservation or violation for the IW near the bilayer, one has to systematically analyze the breakdown temperature for the IW molecules. This investigation requires lipid bilayers at different phases at different temperatures which merits stand alone investigations in future. However, all classes of IW molecules are not fitted to the previous KWW function due to the appearance of a long time tail very similar to that for the IW molecules near proteins [Marzio *et al.*, 2016]. The SISF of IW molecules can be fitted for with three relaxation time-scales where one more stretched parameter is added to the KWW function as

$$F_s(q,t) = (1 - f_Q - f_Q^{'})exp\Big( - \Big(\frac{t}{\tau_s}\Big)^2\Big) + f_Q exp\Big( - \Big(\frac{t}{\tau_\alpha}\Big)^{\beta^\alpha}\Big) + f_Q^{'} exp\Big( - \Big(\frac{t}{\tau_l}\Big)^{\beta^l}\Big) \tag{4.2}$$

$\tau_l$ and $\beta_l$ are longer relaxation time and stretching parameter respectively. Although such stretched long relaxation is not so common in glass-former liquids, similar $\tau_l$ for the IW molecules near

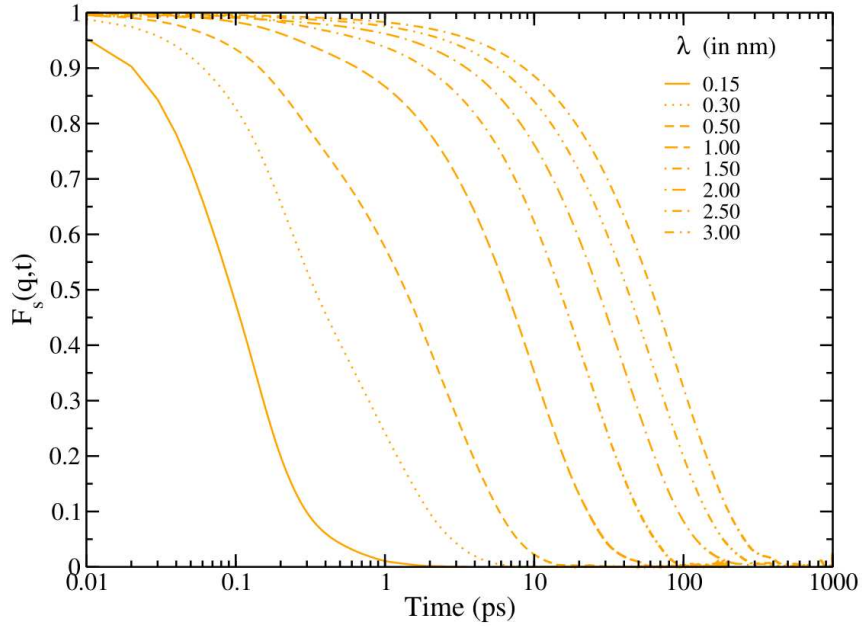


Figure 4.8: SISF of BW at $\lambda$ values ranging from 0.50 nm to 3.00 nm.

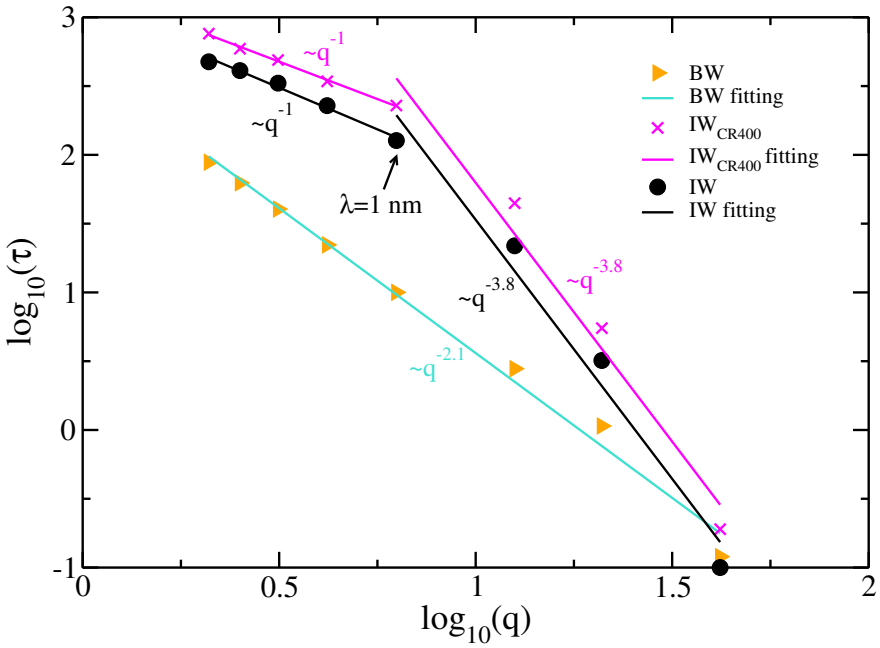


Figure 4.9: log($\tau$) vs log(q) plot for BW, $\mathrm{IW_{CR400}}$ and IW. Solid lines: fitting.

Table 4.2: Fitting parameters of SISFs for all classes of IW and BW. Correlation coefficients are >0.99. The relaxation times of IW ($\tau_l$) and BW ($\tau_\alpha$) are compared with literature showing the suitability of Berger force fields in combination with TIP4P/2005 water model.

| Region | $\tau_s$ (ps) | $f_Q$ | $\tau_\alpha$ (ps) | $\beta_\alpha$ | $f'_Q$ | $\beta_l$ | $\tau_l$ (ps) | $\tau_{HB}$ (ps) |
|---|---|---|---|---|---|---|---|---|
| IW | 0.29 | 0.23 | 2.87 | 0.99 | 0.71 | 0.48 | 15.26 | 14.96 |
| IW-IW | 0.21 | 0.36 | 2.69 | 0.92 | 0.55 | 0.59 | 20.93 | 14.96 |
| IW-CO | 0.32 | 0.21 | 2.86 | 0.99 | 0.75 | 0.46 | 15.03 | 16.74 |
| IW-Glyc | 0.31 | 0.20 | 2.74 | 0.92 | 0.77 | 0.45 | 15.12 | 18.96 |
| IW-PO | 0.29 | 0.26 | 2.69 | 0.91 | 0.69 | 0.48 | 15.15 | 13.00 |
| $IW_{CR400}$ | 0.17 | 0.22 | 2.72 | 0.82 | 0.70 | 0.68 | 85.31 | 122.85 |
| BW | 0.24 | 0.88 | 2.53 | 0.93 | | | | 3.98 |
| Reported literature ($\tau_l$-IW and $\tau_\alpha$-BW) | | | | | | | | |
| IW | Simulations | $\approx$ 10.00 ps [Magno and Gallo, 2011] | | | | | | |
| | | | | | | | | |
| BW | Simulations | $\approx$ 1.00 ps [Magno and Gallo, 2011] | | | | | | |

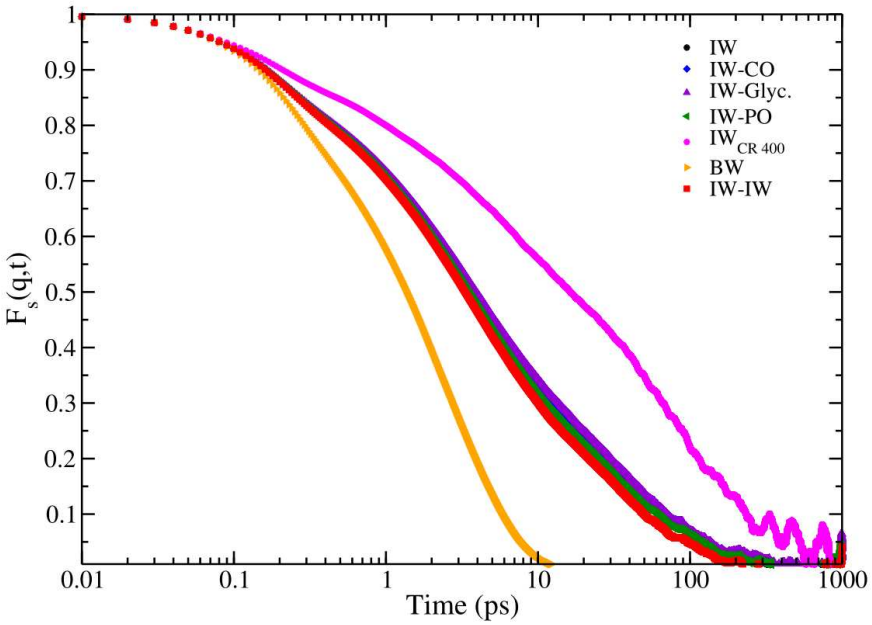


Figure 4.10: SISF for all classes of IW and BW at $\lambda = 0.50$ nm.

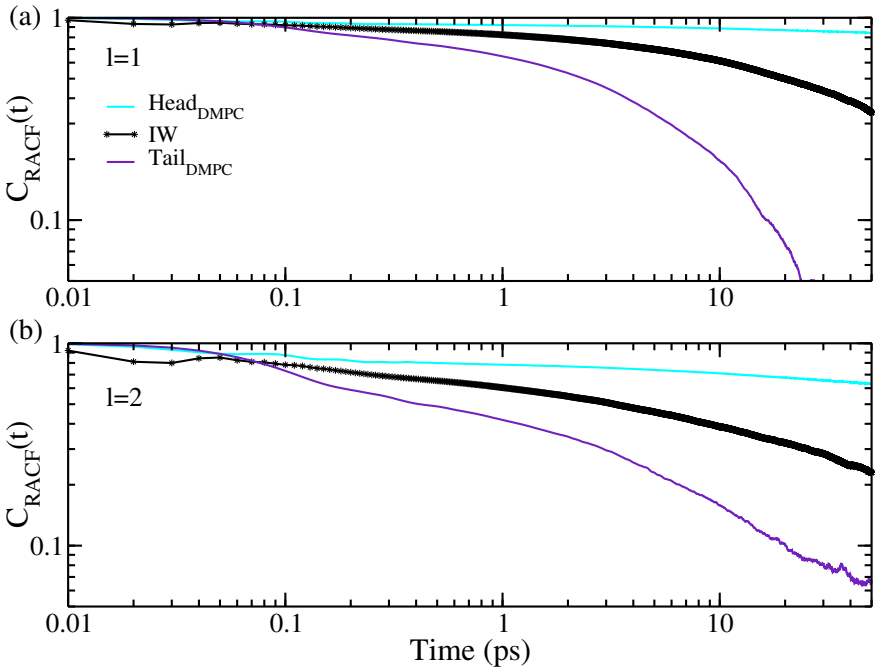


Figure 4.11: RACF for a) first and b) second order Legendre polynomial for lipid head, tail and IW.

Table 4.3: Reorientational correlation relaxation time scales for lipid head, tail and IW. All correlation coefficients were >0.99.

| | Region | $A_f$ | $\tau_f$ (ps) | $A_s$ | $\tau_s$ (ps) |
|---|---|---|---|---|---|
| l=1 | Head$_{DMPC}$ | 0.09 | 50 | 0.90 | 637.07 |
| l=2 | | 0.10 | 50 | 0.75 | 252.06 |
| l=1 | Tail$_{DMPC}$ | 0.48 | 2.75 | 0.36 | 14.32 |
| l=2 | | 0.25 | 1.01 | 0.40 | 11.94 |
| l=1 | IW | 0.25 | 6.51 | 0.62 | 83.26 |
| l=2 | | 0.29 | 3.05 | 0.42 | 77.83 |

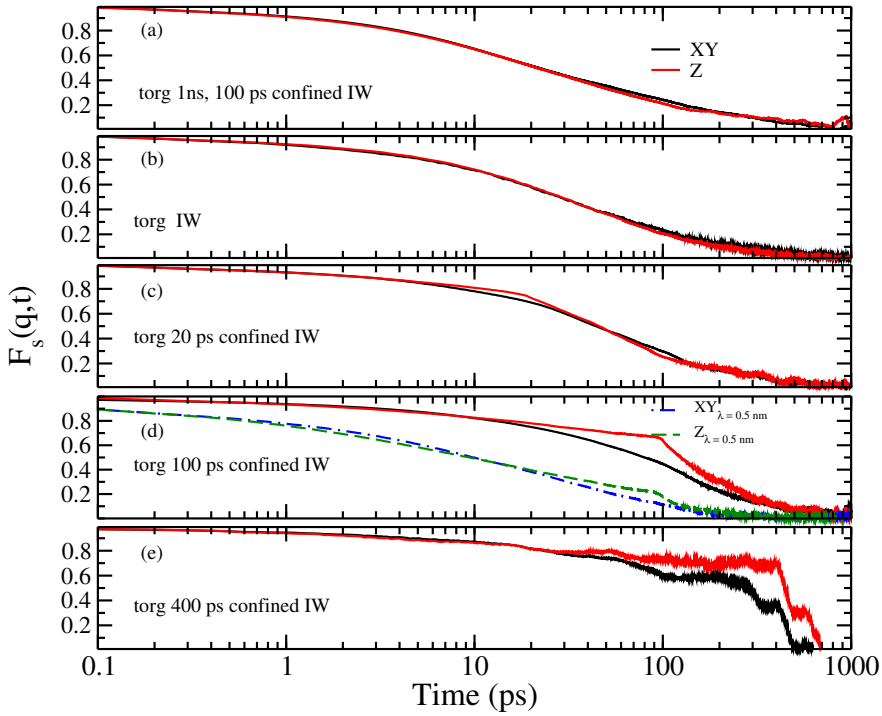


Figure 4.12: $F_s(q,t)$ of IW calculated along xy and z at $\lambda = 1$ nm. Time origins (torg) are averaged in two ways : a) torg over entire 1 ns run length for continuously residing IW for 100 ps, b)-e) torg over confinement time. b) IW for any frame, c) continuously residing IW for 20 ps, d) continuously residing IW for 100 ps at $\lambda = 1$ nm and $\lambda = 0.50$ nm and e) continuously residing IW for 400 ps.

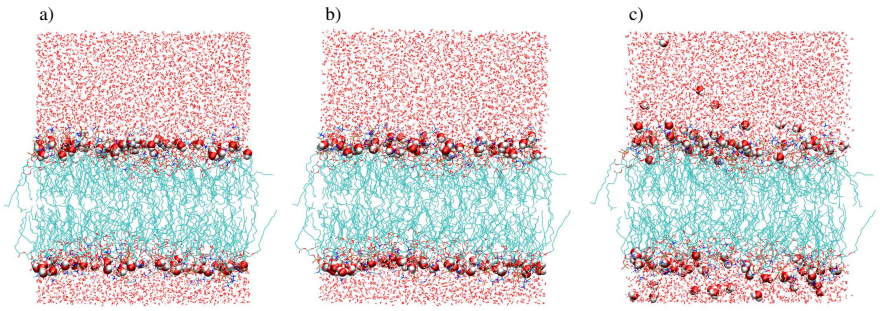


Figure 4.13: Snapshot of the DMPC bilayer at a) 50 ps, b) 100 ps and c) 150 ps. IW: CPK representation in red and white, DMPC lipids : line representations in cyan blue, remaining water : red dots.

proteins is known to follow Arrhenius dependence on temperatures with a cross-over due to the protein structure fluctuations [Marzio *et al.*, 2016]. $\tau_s$ and $\tau_\alpha$ of all classes of IW show similar time-scales (table 4.2) as that of the BW and consistent with the time-scales obtained for hydration water near protein or sugar [Magno and Gallo, 2011; Marzio *et al.*, 2016].
To check the wavelength dependence of the slowest relaxations, log-log plot of the slowest relaxations and q are shown in figure 4.9. The slowest relaxation time ($\tau_\alpha$) follows a quadratic dependence on the q for the BW. The wavelength dependence of $\alpha$-relaxation time-scales ($\tau_\alpha$) is generally characterized by the exponential decay of $F_s(q,t) = exp(-Dq^2t)$ at all wave lengths at room temperature. So the SISF of the BW have a $q^{-2}$ dependence. In contrast, the slowest relaxation time of both IW and $\mathrm{IW_{CR400}}$ deviate from quadratic dependence indicating non-diffusive dynamics as seen earlier for liquids while supercooling [Bhattacharyya *et al.*, 2010]. However, the deviation from quadratic dependence on q for IW and $\mathrm{IW_{CR400}}$ is non-monotonic in nature. There are cross-overs from linear to quadratic behavior at $\lambda = 1$ nm for both IW and $\mathrm{IW_{CR400}}$. The non-diffusive dynamics of IW is influenced by confinement above a length-scale of 1 nm probably because the thickness of the interface layer is 0.6 nm along z, by definition.
SISF of the IW and the BW molecules are compared in figure 4.10 for $\lambda = 0.5$ nm which is slightly greater than the location of the first peak (0.3 nm) of the g(r) of water oxygens. This value of $\lambda$ is chosen so that by this length scale all fast and slow relaxations of the IW molecules are over. Moreover, the differences in SISF between IW and BW are more prominent for $\lambda = 0.5$ nm than for $\lambda = 0.3$ nm. The IW-CO/IW-Glyc exhibit the slowest $\tau_s$ and $\tau_\alpha$ since they are buried towards the hydrophobic region of the lipids. Interestingly, the $\tau_s$ and the $\tau_\alpha$ for $\mathrm{IW_{CR400}}$ are 10 orders of magnitude slower than the remaining classes of water. However, all classes of water follow a long time stretched exponential tail (described by $\tau_l$) which is clearly absent in the BW. Notably, the $\tau_l$ for $\mathrm{IW_{CR400}}$ is $4-6$ times larger than that for the remaining classes of IW molecules since they reside in the hydration layer for a longer time window. The emergence of $\tau_l$ is attributed to the very slow relaxation of the IW molecules arrested in a cage of hydrogen bond networks formed near the lipid head groups. To understand the physical origin of such stretched relaxation of IW molecules, intermittent hydrogen bond auto-correlation functions ($\mathrm{C}_{HB}(\mathrm{t})$) of IW molecules are calculated using

$$C_{HB}(t) = \frac{< h_{IW-HG}(0) h_{IW-HG}(t) >}{< h_{IW-HG} >} \tag{4.3}$$

where $\mathrm{h}_{IW-HG}(\mathrm{t})$ and $\mathrm{h}_{IW-HG}(0)$ represent hydrogen bonds between IW molecules and head-groups (HG) at time t and 0 respectively. $\mathrm{h}_{IW-HG}$ is 1 when a hydrogen bond is formed between the IW molecules and the HG and is 0 otherwise. Using reactive flux correlation analysis [Pasenkiewicz-Gierula *et al.*, 1999; Luzar, 2000], hydrogen bond relaxations ($\tau_{HB}$) are calculated from the forward rate constants of hydrogen bond breaking reactions for all classes of IW discussed in the previous chapter. The hydrogen bond relaxations range from $13-19$ ps for IW-PO/IW/CO/Glyc [Srivastava and Debnath, 2018] and are very close to the values of $\tau_l$ mentioned in table 4.2. The hydrogen bond relaxation of $\mathrm{IW_{CR400}}$ is found to be $\sim 100$ ps which is again very close to the $\tau_l$ presented in table 4.2. Since the time-scales of $\tau_l$ for the IW molecules match well with their hydrogen bond relaxations ($\tau_{HB}$ in table 4.2), the hydrogen bond dynamics of the IW molecules can be the physical source of such long relaxations.
Earlier, bound water molecules are found to exhibit two time-scales, the fastest time-scale is connected to the BW dynamics and the slowest time-scale is found to be hydrogen bond relaxation time-scale [Nandi and Bagchi, 1997; Pal *et al.*, 2002]. However, translational MSD and rotational relaxations of lipid heads and tails are not straightforwardly connected to the MSD and rotational relaxations of the IW molecules (figure 4.11 and table 4.3). The rotational relaxation time-scales of lipid tails are closer to the relaxation time scale of IW molecules where the rotational time-scales of lipid heads are one order of magnitude slower than that of the IW molecules (table 4.3). This indicates that relaxations of the IW molecules are not governed by the relaxations of the lipid heads which are hydrogen bonded to the IW. The exact dependency between lipid and IW relaxations thus needs further intensive investigations.
Although, relaxations of $\mathrm{F}_s(\mathrm{q,t})$ shown in figure 4.10 capture the interlayer dynamics well through

hydrogen bond dynamics, the effect of confinement is not visible in the relaxations. This is because SISF in figure 4.10 is calculated at $\lambda = 0.5$ nm, a distance within the interface layer thickness (0.6 nm along the bilayer normal, z). $F_s$(q,t) at $\lambda = 1$ nm (a distance larger than the layer thickness) (figure 4.12) a)) has a $\tau_l$ value close to the confinement lifetime ($\sim$ 76 ps) and $\tau_\alpha$ close to the hydrogen bond lifetime ($\sim$ 14 ps). However, the dynamics along xy and z are similar in nature. If IW molecules are probed at any time frame which may not reside in the layer for a finite time-span they too exhibit similar dynamics along xy and z (figure 4.12 b)) where the slowest relaxation time-scale is similar to their confinement lifetime ($\sim$ 82.25 ps). Survival probability of IW shows two time-scales (fast and slow, table 2.4) indicating distributions in lifetime for IW. If IW molecules which are continuously residing for $\sim$ 20 ps (close to its fastest survival time of $\sim$ 16.4 ps) are probed and averaged over time-origins ($t_{org}$) only over 20 ps, $F_s$(q,t) along z relaxes slower than $F_s$(q,t) along xy and the effect of confinement along z is clearly visible at $\sim$ 20 ps (figure 4.12 c)). The difference in xy and z is more prominent for IW continuously residing for 100 ps (figure 4.12 d)). Similar differences along xy and z are observed for SISF calculated at $\lambda = 0.50$ nm when averaged over torg only over 100 ps (figure 4.12 d)). The sudden drop of $F_s$(q,t) along z near 100 ps is because only those IW are probed which are confined in the interface layer along z continuously for 100 ps. These molecules relax very fast after the confinement lifetime. This is evident from the snapshots of the bilayers shown in figure 4.13. For the initial 50 ps, IW are residing at the layer, and at 100 ps the same molecules are still residing in the same layer, however at 150 ps, the same molecules are scattered to the bulk. So the movement of the IW for the initial 100 ps is more restricted than the next 50 ps along z when they no longer reside in the interface. Diffusion of the IW from interface to bulk just after the confinement lifetime is very fast with a high probability. This results in a sudden drop in $F_s$(q,t) along z. The effect of confinement on $F_s$(q,t) is examined for $IW_{CR400}$ with a confinement lifetime of 400 ps. A similar drop in $F_s$(q,t) is found near their confinement lifetime of 400 ps (figure 4.12 e)).

## 4.8 VAN HOVE CORRELATION FUNCTIONS FROM BLOCK ANALYSIS

A block analysis approach is used to calculate the heterogeneity length scale present in the IW molecules at the membrane-water interface. The bilayer surface is divided into boxes of length $L_B$ where $((L/L_B)^d)$ is the total number of boxes considered, L is the total boxlength and d is spatial dimension. To obtain sufficient statistics to evaluate the length scale associated with the dynamical heterogeneity [Karmakar *et al.*, 2009; Avila *et al.*, 2014; Chakrabarty *et al.*, 2017], one needs a large system size. Equilibration of such a large membrane using an all atom molecular dynamics simulation is expensive and thus we can reach a system size $\sim$ 4 times larger than our initial system size with a box-size of $12.6 \times 12.6 \times 7.7$ nm$^3$. The coarse grained displacement of one block is calculated by,

$$\Delta x_j^B(\tau) = \frac{1}{n_j} \sum_{i=1}^{n_j} [x_i(\tau) - x_i(0)] \tag{4.4}$$

where $n_j$ is the number of IW molecules in the $j^{th}$th block. The blocked van Hove function is defined as,

$$G_s^B(x,\tau) = \left\langle \frac{1}{N_B} \sum_{j=1}^{N_B} \delta[x - \Delta x_j^B(\tau)] \right\rangle \tag{4.5}$$

$G_B^s(x,t)$ for each block is calculated with a time interval of 0.3 ps by which IW enter in the sub-diffusive regime. By considering different values of $L_B$ , $G_B^s(x,t)$ of each block is calculated for 1 ns run-length averaging over 99970 time frames and shown in figure 4.14. With increase in $L_B$, the non-Gaussian distribution slowly becomes more and more Gaussian. A crossover from non-Gaussianity to Gaussianity is obtained at a coarse grained box length of 5.5 nm (figure 4.14)

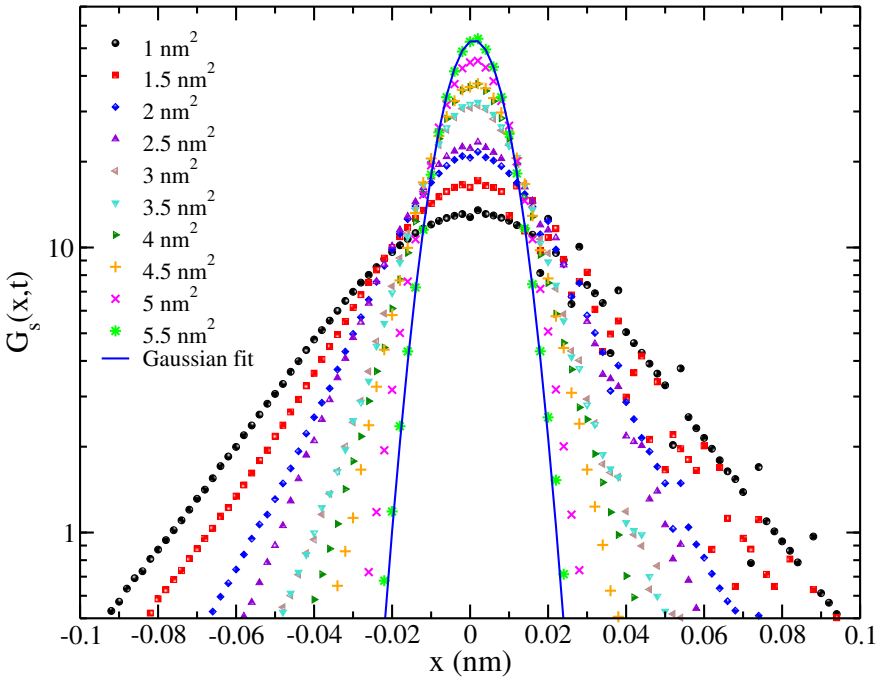


Figure 4.14: One dimensional van Hove correlation function for different coarse grained length scales. Solid blue line showed Gaussian fitting for coarse grained block area of $5.5 \times 5.5$ nm$^2$.

indicating the length-scale associated with the spatial heterogeneity in confined water. Although dynamics of water is expected to have a cross-over from non-Gaussian to Gaussian distribution once the numbers of particles increase to a large number with larger blocks according to the central limit theorem, block analysis enables one to predict the length-scale of the transition to Gaussianity which does not naturally come by central limit theorem. The length-scale of dynamical heterogeneity obtained from block analysis is examined earlier for different temperatures for glass-former liquids and compared with other independent methods [Bhowmik *et al.*, 2018].

To find the physical relevance of the heterogeneity length-scale of the confined water to the membrane structure, tilt of the tail to head vectors of the lipids [Schmid, 2013; Debnath *et al.*, 2014; Bradley and Radhakrishnan, 2016; Terzi and Deserno, 2017] are calculated as functions of lipid head group (x,y) coordinates on the bilayer surface using the following equation,

$$t(x,y) = cos^{-1}\frac{\vec{r}.\vec{n}}{\mid \vec{r} \mid} \tag{4.6}$$

where $\vec{r}$ is the tail to head vector of the lipid chain and $\hat{n}$ is the bilayer normal. A fast Fourier transform of t(x,y) provides the spectral intensity, and t(q) which is plotted on the xy plane of the membrane surface and shown in figure 4.15 a). The q value corresponding to the highest peak in figure 4.15 b) denotes the wave vector associated with the weak undulation of the membrane. Similar representative weak undulation is demonstrated in the side view of the bilayer snapshot in figure 4.15 c). The q vector of 1.14 nm$^{-1}$ corresponding to the highest spectral intensity provides the wavelength ($\lambda = \frac{2\pi}{q} = 5.51$ nm) of the weak undulation.

The wave-length (5.51 nm) of the weak undulation of the bilayer obtained from intensity spectra of lipid tilts is similar to the dynamical heterogeneity length-scale (5.5 nm) of the IW molecules obtained by the block analysis approach. Although tilt is a small length-scale membrane undulation phenomenon unlike curvature, it has been recently shown that the bending and tilt modulus can be extracted from lipid longitudinal and transverse director fluctuations [Watson *et al.*, 2012; Terzi and Deserno, 2017; Chaurasia *et al.*, 2018]. Thus our finding suggests that the heterogeneity length-scale of interfacial water can be related to the small wavelength fluctuations of a fluid membrane. To

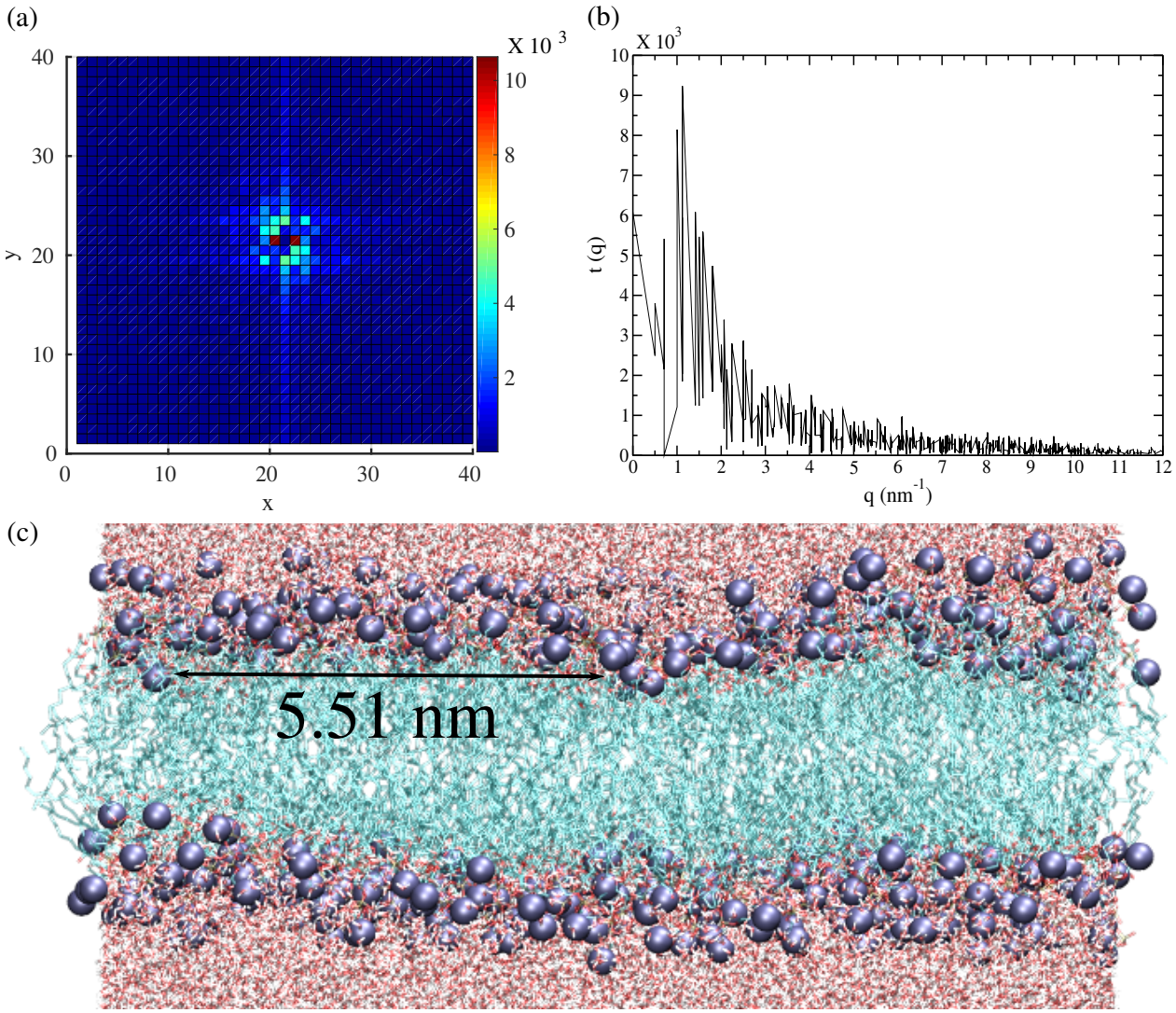


Figure 4.15: a) Top view of spectral intensity of DMPC tilt plotted on bilayer x-y plane showing emergence of peaks. x and y indicate the grids present on the surface and thus has no units. b) The spectral intensity t(q) vs $q$ shows the q value with the highest intensity at 1.14 $nm^{-1}$. c) Side view of DMPC lipid bilayer showing the length scale of the local weak undulation of the lipid membrane.

put the observation on a strong ground, one has to extensively investigate the correlation between heterogeneity length scale and undulation wavelength of a rippled bilayer where the curvature is prominent. The correlation of dynamical heterogeneity length scale of the confined water with the wave-length of the weak undulation of the membranes indicates a tantalizing possibility of length-scale prediction from the phase of a membrane.

## 4.9 SUMMARY

In summary, this chapter provides evidence of spatio-temporal heterogeneities in interface water near lipid membranes at temperature well above room temperature using all-atom molecular dynamics simulations. Water molecules continuously residing in the interface layer for a time window of 100 ps are identified as IW. To investigate the influence of chemical confinement on their dynamics, the IW molecules which form hydrogen bonds to another IW molecule or to CO/PO/Glyc. lipid head groups for at least one time frame within their confinement time window are identified and referred to as IW-IW/CO/PO/Glyc. Dynamics of these different classes of water is relevant in understanding the structural or orientational heterogeneity of interface water near zwitterionic PC lipids or cationic or anionic lipid/surfactant interfaces previously reported using SFG spectroscopy and molecular dynamics simulations[Roy *et al.*, 2014; Inoue *et al.*, 2017; Cyran *et al.*, 2018]. The non-Gaussian parameters of all classes of IW molecules show $\beta$ to $\alpha$ relaxations at similar spatio-temporal scale where their respective mean square displacements leave the sub-diffusive regions. IW-CO/Glyc. being buried deepest towards the hydrophobic core of the membrane have slowest $\beta$ to $\alpha$ relaxations among all classes of IW. The slowest relaxation of IW-CO/Glyc. is attributed to the presence of a strong barrier of the membrane for water and ions at a location close to carbonyl head groups as seen in time-resolved fluorescence study [Koehorst *et al.*, 2010]. Such slow relaxations of IW are signatures of dynamical heterogeneities commonly found in glass former liquids [Kob *et al.*, 1997]. In contrast, the non-Gaussian parameter of bulk water molecules (BW) asymptotically decays to zero with a faster $\beta$ to $\alpha$ relaxation exhibiting underlying Fickian dynamics. To understand the influence of confinement lifetime on the dynamics of IW, another class of IW molecules are identified which continuously reside in the interface layer for a longer time of 400 ps and are referred to as $\mathrm{IW_{CR400}}$. Since $\mathrm{IW_{CR400}}$ has the longest confinement lifetime, more profound dynamical heterogeneities are observed for these molecules. The $\beta$ to $\alpha$ relaxation time scales of all classes of IW molecules are found to be closer to their confinement lifetimes.

The translational self part of the van Hove correlation function calculated at a time-interval of $\beta$ to $\alpha$ relaxation time of NGP shows significant deviations from Gaussianity for all classes of IW. IW-Glyc. has the highest peak in the radial van Hove correlations among all classes of IW molecules very similar to their relaxations in NGP. $\mathrm{IW_{CR400}}$ with longest confinement lifetime has very few IW molecules inhomogeneously distributed over the bilayer surface. The inhomogeneous distribution can cause rattling or hopping of IW molecules between cages which are not spatially close leading to a peak and a shoulder in the radial van Hove correlation function. Since the bilayer is symmetric along the surface, one-dimensional van Hove correlation functions are calculated for all classes of water molecules at time-intervals having very similar values of MSD on the surface. BW follows a Gaussian fit in the one-dimensional van Hove correlation function where all classes of IW molecules show a significant amount of deviations. The exponential tails of the one dimensional van Hove correlation function are universal signatures of dynamical heterogeneity [Chaudhuri *et al.*, 2007; Sengupta and Karmakar, 2014] and are originated from the waiting time distributions for subsequent hopping transitions between cages formed by neighboring IW molecules hydrogen bonded to each other. Self intermediate scattering functions of all classes of IW molecules exhibit three well separated time scales unlike BW : fast ballistic motion in a cage, intermediate hopping transitions between neighboring cages and eventual relaxation of the cage. Although the long time cage relaxations are not so common in glass forming liquids, similar long relaxations are obtained for IW molecules near protein due to protein structure fluctuations [Camisasca *et al.*,

2016]. The long time relaxations of all classes of IW molecules are in excellent agreement with the respective hydrogen bond relaxations calculated from reactive flux correlation analysis [Srivastava and Debnath, 2018]. This confirms that the dynamical heterogeneity of IW molecules is originated from relaxation of hydrogen bonds due to hydrogen bond breaking irrespective of the confinement lifetime or the nature of the chemical confinement. To capture the confinement lifetime in the slowest relaxations, SISF should be calculated for a wavelength larger than the interface layer thickness. Importantly, the translational mean square displacement and rotational correlation functions of IW molecules are not straightforwardly coupled to that of the lipid heads or tails. However, this opens up a new direction to investigate the coupling between lipid and IW molecule dynamics in more detail.

The length scales of spatially heterogeneous dynamics are measured from van Hove correlation functions of IW molecules employing a block analysis approach. The IW molecules are coarse-grained over blocks of varying sizes on the membrane surface and one dimensional van Hove correlation functions are calculated for those blocks. A cross-over from non-Gaussianity to Gaussianity in van Hove correlation functions of IW molecules is found to occur at a specific length-scale which is identified as the dynamical heterogeneity length-scale of the IW. The spectral intensity calculated from the tilt of the lipids on the membrane surface estimates the wave-length of the weak undulations of the membrane in the fluid phase. The wave-length matches well with the dynamical heterogeneity length scale obtained from block analysis approach suggesting a correlation between the heterogeneity length scale and the membrane undulations. This correlation can be more profound for a membrane surface with a strong curvature which can be examined for a membrane in a rippled phase. Thus, we suggest an influence of the membrane phase on the length scale of dynamical heterogeneity of confined water, which merits further stand alone investigations.

Our calculations reveal that the slow relaxations of chemically confined water molecules near lipid membranes are governed by dynamical heterogeneities originated from hydrogen bonds rather than the dynamics of physically close lipid head groups. Moreover, the length-scale dependence of dynamical heterogeneity of confined water is predicted using the block analysis of the van Hove function. Importantly, the information of length-scale of dynamic heterogeneities is found to be possibly embedded in the length-scale of the lipid phase through its curvature. Thus the analyses can attempt to predict a length-scale for the membrane phase transition in future. Since confined biological water near membranes at room temperature exhibits similar dynamics to the super-cooled bulk water, the results can enhance our understanding of the mechanisms of bioprotection during freezing stresses and will be useful for mimicking cryo-preservation techniques at room temperature.

At the same time, our findings raise a few more questions : how strongly are the lipid dynamics coupled to the water dynamics? Is the coupling significant enough to influence the dynamics of lipids generating rafts, or skeleton fences? [Munro, 2003; Lingwood and Simons, 2010; He *et al.*, 2016] Is it relevant to the phase transitions of lipid bilayers?